Pipe pile installation effects in soft clay

Article *in* ICE Proceedings Geotechnical Engineering · January 2006

DOI: 10.1680/geng.2006.159.4.285

3 authors, including:

Xiangtao xu

13 PUBLICATIONS **562** CITATIONS

SEE PROFILE

Barry Michael Lehane

University of Western Australia

211 PUBLICATIONS **5,090** CITATIONS

SEE PROFILE

Field measurements during pipe pile installation in soft clay

X. Xu[1]

B.M. Lehane[2]

H. Liu[3]

[1] PhD student, School of Civil & Resource Engineering, Univ. of Western Australia

[2] Associate Professor, School of Civil & Resource Engineering, Univ. of Western Australia

[3] Professor, GeoHohai, Hohai Univ., Nanjing, China P.R.

Corresponding author: Ms Xiangtao Xu
School of Civil & Resource Engineering
University of Western Australia
Crawley, Perth WA 6009
AUSTRALIA

SUMMARY

The shortage of field measurements to examine existing predictive methods for pipe piles in clay prompted an experimental programme in Shanghai, China, in which displacements and stresses were measured in the vicinity of pipe piles during their installation in a soft lightly overconsolidated clay. The test programme was also conducted to assist assessment of the installation effects associated with a recently patented pile, referred to as the PCC pile. The field measurements are compared with existing predictive methods such as Shallow Strain Path and Cavity Expansion methods (SSPM and CEM). The SSPM is shown to be the most suitable for the prediction of ground displacements, although the, more straightforward, CEM, can provide realistic predictions of radial movements when calculations are performed using a solid pile with an area equivalent to that of the annulus of the pipe pile. Installation induced excess pore pressures and changes in lateral total stresses remote from pipe piles are also shown to be well predicted using the same cavity expansion method combined with this equivalent radius. The paper provides verification of an expedient means of assessing installation disturbance due to undrained pipe pile installation.

1. INTRODUCTION

A knowledge of the displacement and stress changes induced in the soil surrounding a driven pile is essential to the development of rational predictive methods for evaluating pile performance. Pestana et al. (2002) presented a review of the previous experimental work in this area, which indicated that, of the reported 25 case histories involving instrumentation for displacement piles in clay, only 3 employed open-ended (pipe) piles. This paper extends the sparse database of measurements for pipe piles by presenting measurements of stress changes (radial total stress and pore pressure) and ground deformations (surface ground displacement and lateral deformations) obtained in the vicinity of two large diameter open-ended pipe piles during their installation in soft alluvium in Shanghai, China. These measurements may be used to advance current understanding of mechanisms associated with pipe pile installation for both single and group pile response.

Predictive methods that aim to model displacement pile installation include large strain finite element (FE) theory, FE re-meshing procedures and FE techniques that de-couple material displacements from nodal point displacements (Zienkiewicz 1984, Kiousis et al. 1988, van den Berg 1991, Ghosh and Kikuchi 1991, Hu and Randolph 1998, Yu et al. 2000, and Lu et al. 2002). These techniques require significant expertise and computing resources for their application and, perhaps more importantly, require good quality data for their verification and refinement. Therefore, in addition to providing data to assist the development of these methods, this paper also examines the potential of other simpler methods that are more amenable to immediate use by geotechnical practitioners. These methods are referred to as the cavity expansion method (CEM) described by Randolph et al. (1979) and the shallow strain path method (SSPM), devised by Sagaseta (1987) and Sagaseta et al. (1997).

2. EXPERIMENTAL DETAILS

2.1 The PCC pile

The experimental results, described here, were obtained using instrumentation located in the vicinity of two 1.02m external diameter, 0.744m internal diameter steel pipe piles. These piles, which are designated Piles A and B, provided the temporary formwork for a new type of cast-in-situ concrete pipe pile, referred to as the PCC pile, which was developed by GeoHohai and patented recently in China (Liu et al. 2002a, Liu et al. 2002b). The steel pipe piles comprised an inner and outer pipe (each with a wall thickness of 8mm) to create a 122mm wide annular void; the two pipes were connected at the pile tip using the detail shown in Fig. 1a. The proprietary construction procedure entails (i) vibro-driving of the temporary steel pipe pile, (ii) pouring concrete into the annular void space of this pipe and (iii) withdrawing the steel pipes. The end result is an un-reinforced concrete pipe pile.

The PCC pile has been used primarily in soft ground improvement applications such as for bridge abutment support piling (BASP) and was developed to assist fast-track developments of expressway and other infrastructure in JiangSu, HuNan and ZheJiang provinces. The PCC pile has a high shaft friction to concrete volume ratio and avoids the need for reinforcement to deal with handling and installation stresses; it therefore offers a cost-effective solution when mainly compression loads need to be resisted. The PCC's adaptability to various poor ground conditions has made it a popular choice since being first employed. Photos showing a group of completed PCC piles and installation of the pipe (formwork) are shown in Figs. 1b and 1c.

2.2 Site and soil conditions

The experimental site is located in a northern suburb of Shanghai on the deltaic deposit of the Yangtze River. The stratigraphy, which is summarised on Fig. 2, comprises a 2m thick layer of coarse-grained fill with some organic deposits overlying a 10m thick deposit of soft very silty clay; this deposit is underlain by older (Pleistocene) stiff clay. As seen on Fig. 2, the soft clay layer has a low to medium plasticity, a liquidity index of ≈1.2 and cone penetration test (CPT) end resistance (q_c) increasing with depth from 470 kPa at 2m to 1450 kPa at 12m. The water level was typically at depth of 1.3m and exhibited minor seasonal fluctuations. The 2m layer of surface fill is believed to have increased the clay's vertical effectives stresses (σ'_{v0}) to values very close to the material's vertical yield stresses (σ'_{vy}) i.e. the soft clay may be considered to be normally consolidated or very lightly overconsolidated.

2.3 Instrumentation

A plan of the instrumentation arrangement used in the vicinity of Piles A and B is provided on Fig. 3. This instrumentation comprised (i) 5 No. survey targets (ST) to allow measurement of ground surface heave and lateral movement, (ii) 3 No. inclinometers (I) to enable lateral ground movements to be assessed, (iii) 6 No. pneumatic piezometers (P) for pore pressure measurement and (iv) 6 No. 105mm wide (spade) pressure cell (TP) to record lateral total stresses. The 70mm diameter inclinometer casings were installed to a depth of ≈14m and were embedded firmly in the very stiff silty clay present at this depth (see Fig. 2); a comparison of the inclinometer data with the surveyed lateral movements at ground level indicated that the inclinometer attained effective fixity (i.e. zero lateral soil movement) at a depth of

14m. The pneumatic piezometers were installed in pre-bored holes to depths of 3m and 6m at the centre of 1m high sand response zones, which were sealed top and bottom using a thick layer of bentonite pellets. The total pressure were installed to their target depths of 3m, 6m and 9m by pushing them a distance of 1m below the base of pre-drilled boreholes.

It is noteworthy that the instrumentation was located at a minimum radial distance from the pile centres of two pile radii i.e. the programme of tests focused on obtaining information of the displacement and stress changes in the soil mass surrounding the piles, but not at (or close to) the pile shaft. It was felt that such measurements, combined with static load tests on individual PCC piles, would improve understanding of the performance of PCC pile groups, as well as providing an indication of the effects of adjacent PCC pile installation on a recently cast PCC pile.

2.4 Pile installation

Piles A and B were installed using a vibratory driver (type 110Y-58T). Installation was halted temporarily at tip depths of 3m, 6m, and 9m to allow all instrumentation to be recorded. Piles A and B were installed to final tip depths (L) of 12m and 13.5m respectively and the instrumentation readings were also obtained immediately on attaining these penetrations. The soil plug length was monitored during each pause in driving and was found to be typically 100mm above ground level i.e. installation occurred in a fully unplugged (or coring) mode. It normally took around 10 mins to take all the measurements during each pause and, as a consequence, the total pile installation time was about 45 mins and over 30 mins longer than that of a standard PCC pile in these soil conditions.

3. EXISTING SIMPLIFIED PREDICTIVE TECHNIQUES

The data recorded during installation of the pipe piles in Shanghai are compared with two predictive methods (i) the cavity expansion method and (ii) the shallow strain path method. The main features of these approaches are first described before examining their ability to predict the observed displacements, pore pressures and radial effective stresses remote from the piles.

3.1 Cavity Expansion Method (CEM)

The cavity expansion method (CEM), applied to piles, assumes that during pile installation, the soil (away from the influence of the pile tip and ground surface) is displaced in a similar manner to the soil adjacent to an expanding cylindrical cavity. The stress changes are predicted using cylindrical cavity expansion closed-form solutions (e.g. Butterfield & Bannerjee 1970), numerical finite element solutions (e.g. Randolph et al. 1979) or the results from *in situ* pressuremeter tests. Although Baligh (1985), and many others, have shown that the CEM does not predict realistic strain histories of elements in the vicinity of a displacement pile (and hence can lead to gross errors in predicted pile shaft shear stresses). Lehane & Gill (2004) show, nonetheless, that it provided good estimates of total radial displacements (δ_r) induced during installation of six separate closed-ended piles in different clays. The CEM expression for δ_r, for soils at initial radius r, is given by:

$$\frac{\delta_r}{R} = \sqrt{1+\left(\frac{r}{R}\right)^2} - \frac{r}{R} \qquad (1)$$

Randolph (2003) indicates that the corresponding expression to Equation (1) for pipe piles, with an inner radius of r_{inner}, is:

$$\frac{\delta_r}{r_{eq}} = \sqrt{1 + \left(\frac{r}{r_{eq}}\right)^2} - \frac{r}{r_{eq}} \qquad (2a)$$

$$r_{eq} = \sqrt{R^2 - r_{inner}^2} \qquad (2b)$$

where r_{eq} is the radius of an (equivalent) closed-ended pile that gives the same volume of displaced soil. Equation (2) assumes that pipe piles installation occurs in a fully coring mode and that all the soil beneath the annular tip is displaced laterally. Such an assumption requires validation using field measurements (Randolph 2003).

The strain path method indicates that cavity expansion strains predominate outside of the large strain region close to the pile shaft. The database compiled by Lehane & Gill (2004) also showed that total vertical displacements at $r/R \geq 2$ are negligible compared to the total radial displacements. Therefore, although soil unloading effects as the pile tip advances below any given level can have a significant effect on the effective stress regime, it is possible that the CEM may provide an expedient way of predicting the excess pore pressures and total stress changes remote from a displacement pile after installation. The ability of the following simple expression for excess pore pressure (Δu) proposed by Randolph (2003) based on the Gibson & Anderson (1961) cavity expansion solution in an elastic perfectly-plastic clay, will be compared with the Shanghai pipe pile data:

$$\frac{\Delta u}{s_u} = \ln\left(\frac{\rho G}{s_u}\right) - 2\ln\left(\frac{r}{R}\right) = \ln\left(\frac{G}{s_u}\right) - 2\ln\left(\frac{r}{r_{eq}}\right) \geq 0 \qquad \rho = 1 - \left(r_{inner}/R\right)^2 \tag{4}$$

where G is the clay's (equivalent linear) shear modulus, s_u is the undrained shear strength, G/s_u is the rigidity index (I_r) and ρ is the area ratio, which varies from zero to unity for a closed-ended pile. Equation (4) predicts that the maximum excess pore water pressure surrounding a pipe pile will be $s_u \ln(\rho)$ lower than that of a closed ended pile of the same outer radius.

The CEM predicts that that the soil adjacent to the pile shaft is at a critical state under plane strain conditions with a radial major principal stress. The radial effective stress, immediately after installation assuming a Coulomb failure criterion is then given by Randolph et al. (1979) as:

$$\sigma'_{ri} = \left[1 + \sqrt{3/M}\right] \times s_u \quad \text{with } M = 6\sin\phi'/(3 - \sin\phi') \quad \text{for } R < r < r_p \tag{5a}$$

$$\sigma'_{ri} = K_0 \sigma'_{v0} \qquad \text{at } r > \approx 10\ R \tag{5b}$$

where r_p is the radius of the plastic zone, which for an elastic perfectly plastic clay, is given:

$$r_p / R = \sqrt{G/s_u} \tag{5c}$$

A large body of experimental data collated by Bond (1989) and Lehane (1992) for closed-ended piles indicates that equation (5) can over-predict σ'_{ri} close to the pile shaft by a factor of 10 in low OCR, very sensitive clays; such an over-prediction arises

because the CEM does not capture the large installation imposed shear strains and consequent softening of clay close to the pile shaft.

3.2 Shallow Strain Path Method (SSPM)

The shallow strain path method (SSPM) is an extension of the strain path method (SPM) developed by Baligh (1985). The SSPM and SPM assume that, during pile installation, the soil moves relative to the pile tip in the same way that an incompressible, inviscid fluid would flow around the tip and that this flow is independent of the shearing resistance of the soil. The flow streamlines are used to determine the strain paths for all elements surrounding the pile, which may then be used to calculate effective stresses using an appropriate constitutive model. The SSPM devised by Sagaseta (1987) and Sagaseta et al. (1997) improves on the SPM by allowing for the influence of the free ground surface on the soil response. The SSPM has been successfully applied to the prediction of ground movements caused by undrained closed-ended pile installation e.g. see Sagaseta & Whittle (2001) and Lehane & Gill (2004). For this case, the SSPM gives the following closed form expressions for the radial movement (δ_r) and vertical displacement (δ_z) at the soil surface (at z=0) due to undrained plugged pipe pile installation.

$$\delta_r(\text{closed - ended}) = \frac{R^2}{2} \times \left(\frac{L}{r \times \sqrt{r^2 + L^2}} \right) \tag{6a}$$

$$\delta_z(\text{closed - ended}) = -\frac{R^2}{2} \times \left(\frac{1}{r} - \frac{1}{\sqrt{r^2 + L^2}} \right) \tag{6b}$$

The capabilities of SSPM to predict ground movements associated with the installation of the Shanghai piles is examined in the following. However, no closed-form solution exists for the case of an unplugged pipe pile (other than at z=0 and r=0) and it is necessary to use numerical integration of the soil 'velocities' to predict displacements. According to SSPM, the velocity field for a pile tip at a depth z=L below the surface can be derived by considering a ring or annular source discharging a volume, V, at z=L. As described by Sagaseta (1995), the velocity is obtained by combining three components due to (i) a ring source, S, within an infinite/full space (ii) a ring sink, S', absorbing an equal and opposite volume to the source (i.e. –V) located at an elevation z= -L above the ground surface and (iii) a distribution of corrective shear tractions applied to the surface to simulate a stress free surface.

Prediction of stress changes and pore pressure using the SSPM is far less straightforward than for the CEM and does not fall under the category of simplified methods discussed in this paper.

4. FIELD MEASUREMENTS AND PREDICTIONS

4.1 Ground heave

The ground heave measured at various normalised radii (r/R) from Piles A and B during their installation are presented as a function of pile embedment length, L, in Fig. 4. Both the ground heave and pile embedment length are normalised by the average pile radius R (510mm). It is apparent that the ground heave increases at a decreasing rate with L/R and tends to a constant value at a fixed r/R location when L/R ratios exceed

about 20. It is also noteworthy that the heave displacements indicated by both piles are closely comparable.

The corresponding predictions of surface ground heave using the SSPM were evaluated by Xu (2004) and are presented as variations of $\delta_z L/R^2$ with r/L on Fig. 5[1]. The measured data are plotted in the same format and are seen to be in very close agreement with predictions; minor deviations from the predicted trend line are evident at r/R=10, where recorded heave displacements were very small and hence more prone to measurement error.

Ground heave displacements predicted using Equation (6b), but using an equivalent pile radius r_{eq} (as given by Equation 2b and equal to 349 mm for the PCC pile) in place of R are also plotted on Fig. 5. The predictions are evidently almost identical to those given by the more involved SSPM calculations for a pipe, indicating that movements remote from the pile are primarily controlled by the volume of clay displaced by the pile. The use of an equivalent solid pile and Equation (6b) therefore provides a simple and effective means of predicting surface heave displacements.

4.2 Surface radial displacement

The normalised surface radial displacements (δ_r/R) measured at various normalised radii (r/R) from Piles A and B during their installation are presented as a function of normalised pile embedment length, L/R, in Fig. 6. The maximum radial displacement induced at r/R=3 is around 12mm. Fig. 7 presents the normalised ground surface radial

[1] Sagaseta & Whittle (2001) explain how the SSPM predicts that, outside the high strain region close to the pile, normalised radial and vertical displacements (δ_r/R and δ_z/R) depend on L/R and that the ratios, $\delta_r L/R^2$ and $\delta_z L/R^2$, vary uniquely with r/L and z/L for any pile geometry (where r is the radius from the pile axis and z is the depth below the ground surface).

displacements in a similar format to that employed in Fig. 5 for the vertical displacements i.e. as $\delta_r L/R^2$ *vs.* r/L. These δ_r values were obtained by tape measurement of the survey targets at fixed location from the piles; see Fig. 3. Also included on Fig. 7 are the predictions obtained using the SSPM technique (by integration of the radial component of the soil 'velocities') for an open-ended pipe pile and using Equation (6a) combined with the equivalent radius of a solid pile (r_{eq}). As before, it is seen that the equivalent solid pile approach gives an identical solution to that of the more involved SSPM calculations. Measured surface radial displacements are, however, significantly lower than predicted values. Such an under-prediction is attributed to the ability of the coarse grained fill, present to a depth of 2m, to change in volume during pile installation (noting that the PCC is vibrated into the ground). The SSPM, which assumes undrained conditions, over-estimates the radial movements significantly, although, as may be inferred from Fig. 5, the actual vertical surface displacements are largely controlled by the (undrained) displacement of the underlying clay.

4.3 Radial displacement below ground level

Radial displacements below ground level were derived from inclinometers assuming fixity of the inclinometer tubes in the very stiff clay at a depth of 14m. The inclinometer casing at a radius of 1m for the centre of pile B was damaged during pile installation and hence, to simplify presentation, only data from inclinometers located adjacent to Pile A are presented here.

The radial/lateral displacements measured at r/R=2, 4 and 7 are plotted on Fig. 8 for four tip penetration depths of Pile A. It may be seen that δ_r values in the fill at shallow

depths are low and consistent with the surface δ_r data on Fig. 7; they are also relatively independent of the pile penetration for L>3m. The displacements are higher in the soft clay layer below the fill and tend to a maximum value at a depth of 4.5m for L≥6m, suggesting perhaps that the clay in this horizon is particularly soft. The attainment of relatively constant lateral displacements in a given soil horizon appears to require a pile tip displacement of about 6m below this horizon. The records on Fig. 8 also indicate that δ_r values reduce by a factor of 10 between r/R=2 and 7.

Lateral displacement profiles predicted using the SSPM are compared on Fig. 9 with measured profiles at two radii (r/R=2 and 7), i.e. at r/R=2 with L=9m and at r/R=7 with L=3m and 9m. For comparative purposes, this figure also includes the CEM solution for lateral displacement obtained using Equation (2).

The SSPM predictions at r/R=7 are evidently in good agreement with measured values at L=3m and L=9m. Unlike the SSPM, the CEM only predicts the final radial movements at large L and these are seen to be considerable over-estimates at L=3. Lateral displacements closer to the pile at r/R=2 with L=9m are, however, under-predicted. Both SSPM and CEM predictions of maximum lateral movements are only about half of the measured peak movements recorded at a depth of 4.5m. It is of interest to note here that Pestana et al. (2002) also observed that the CEM under-predicted peak lateral displacements significantly within about two pile radii of a closed-ended pile in lightly overconsolidated clay.

The CEM predictions for lateral movement obtained using Equation (2) are broadly comparable with the mean measured δ_r values at deep penetration but are typically three times lower than expected assuming a closed-ended pile (estimated by employing

R=510mm in Equation 1). This observation provides further evidence of the predominance of the coring mode of penetration during installation of the piles.

4.4 Pore pressure

Excess pore pressures (Δu) recorded by pneumatic piezometers located at r/R=2, 4 and 7 and the depths (z) of 3m and 6m are plotted on Fig. 10. It is seen that maximum Δu values (Δu_{max}) occur when the tip is close to the level of the pneumatic piezometer but that Δu decreases as the pile tip advances to deeper levels. This reduction may reflect drainage but is probably primarily due to a reduction in mean total stress as the more highly stressed region near the annular tip moves further away.

The radial distributions of Δu_{max} normalised by the free field vertical effective stress (σ'_{v0}) are plotted on Fig. 11 for a range of pile penetrations. $\Delta u_{max}/\sigma'_{vo}$ ratios reduce from 1.2 at r/r_{eq}=2.9 to 0.07 at r/r_{eq}=10, where r_{eq}=349mm for the PCC pile. The CEM prediction of the radial variation of $\Delta u_{max}/\sigma'_{vo}$ was obtained using Equation (4), assuming s_u/σ'_{vo} = 0.3 and a G/s_u value of 150. This prediction is also shown on Fig. 11 and is seen to provide an excellent fit to the measured $\Delta u_{max}/\sigma'_{vo}$ variations.

Validation of the form for Equation (4) is also provided by the $\Delta u_{max}/\sigma'_{vo}$ ratios reported by Pestana et al. (2002) during installation of a closed-ended pile in a soft clay (Youngs bay mud) with a similar OCR to that at the Shanghai test site. These ratios are plotted versus r/r_{eq} (= r/R for a closed-ended pile) on Fig. 11 where they are seen to broadly follow the trend of the CEM predictions and the Shanghai data. $\Delta u_{max}/\sigma'_{vo}$

ratios recorded in St Alban clay with OCR ≈2.2 (Roy et al. 1981) are included on Fig. 11 to highlight the strong influence of OCR on the excess pore pressure field.

4.5 Radial total stress

The radial total stress increases ($\Delta\sigma_{ri}$) recorded during installation at r/R=2 and 4 and at z=3, 6 and 9m are presented as a function of pile embedment length, L, in Fig. 12. It is apparent that $\Delta\sigma_{ri}$ values generally increase with depth and are a maximum when the tip is close to the level of the earth pressure cells. However unlike Δu, the maximum $\Delta\sigma_{ri}$ values reduce significantly as the pile tip penetrates below the level of earth pressure cells. For instance, at r/R=2 and z=3m, $\Delta\sigma_{ri}$ reduces from its maximum value of 94kPa to 29kPa when the pile tip has advanced to 13.5m.

The radial distribution of the maximum changes of total radial stress $\Delta\sigma_{rmax}$ for a range of pile penetrations during pile installation normalised by the free field vertical effective stress (σ'_{v0}) are plotted on Fig. 13(a) assuming a full-displacement closed-ended pile of radius R=510mm and (b) assuming a fully unplugged open-ended pipe pile of equivalent radius r_{eq}=349mm. These distributions are compared with $\Delta\sigma_{rmax}/\sigma'_{v0}$ ratios recorded by McCabe & Lehane (2003) during installation of a closed-ended (precast concrete) pile in Belfast soft clay-silt with OCR ≈1.5. $\Delta\sigma_{rmax}/\sigma'_{vo}$ evidently reduces strongly with increasing radial distance from a pile and, at any fixed radial distance, is larger for the closed-ended pile than for the PCC pipe pile (Fig. 13a). However, if radial distances are normalized by the equivalent pile radius, r_{eq}, the $\Delta\sigma_{rmax}$ data for both the pipe and closed-ended pile fall into a consistent pattern (Fig. 13b). This trend is consistent with that observed for the $\Delta u_{max}/\sigma'_{vo}$ data on Fig. 11 and

supports the contention that both stress and displacement changes remote from a pipe pile can be assessed using solutions for closed-ended piles with a radius equal to r_{eq}.

Equations (4) and (5) may be employed to provide a CEM prediction of the increase in lateral total stress due to pile installation using the equation:

$$\Delta\sigma_{ri} = \left(\sigma'_{ri} - K_0\sigma'_{v0}\right) + \Delta u \qquad (7)$$

This approach, however, leads to a much slower degradation of $\Delta\sigma_{ri}$ with *r* than indicated on Figs. 13a and 13b. A simpler means of assessing $\Delta\sigma_{rmax}$ at some distance from a displacement pile would assume that $\Delta\sigma_{rmax}$ varies in proportion to the CPT q_c value and reduces with the logarithm of r/r_{eq}. Support for this type of approach is provided on Fig. 13c which re-plots the data on Fig. 13b but uses the CPT q_c data rather than σ'_{v0} to normalize the $\Delta\sigma_{rmax}$ data.

4.6 Radial effective stress

Increases in radial effective stress ($\Delta\sigma'_{ri}$) due to the pipe pile installations could be derived from the $\Delta\sigma_{ri}$ and Δu values recorded at two radii (r/R=2 and 4) and at two depths (z =3m and 6m). The values of $\Delta\sigma'_{ri}$ derived in this way at z=6m and r/R=2, together with the corresponding $\Delta\sigma_{ri}$ and Δu data, are normalised by the free field vertical effective stress (σ'_{v0}) and plotted against the relative depth of the pile tip (*h*) on Fig. 14a. The *in situ* K_o value for the lightly consolidated deposit is likely to about 0.55 and therefore this value added to the calculated $\Delta\sigma'_{ri}/\sigma'_{v0}$ ratio yields the effective

stress ratio, $K_i=\sigma'_{ri}/\sigma'_{v0}$. The variation of K_i with h/r_{eq} at r/R=2 and 4 is shown on Fig. 14b for measurements obtained at both z=3m and 6m.

It is of interest to observe that the maximum radial effective stress ratio (K_i) at r/R=2 is recorded close to the level of the pile tip and is about four times the *in situ* K_o value. As is evident on Fig. 14a, radial total stresses reductions with *h* are greater than those of the excess pore pressures and hence K_i reduces as the tip advances below any fixed soil horizon. This relatively rapid decay is in keeping with the trend, proposed by Jardine & Chow (1996), for equalised radial effective stresses acting on the shaft of a displacement pile to vary with $(h/r_{eq})^{-0.2}$ when $h/r_{eq} \geq 8$. For example, recorded K_i values at r/R of 2 and 4 vary approximately with $(h/r_{eq})^{-0.4}$ and $(h/r_{eq})^{-0.25}$ respectively. It should be noted, however, that the K_i values at the pile shaft in the Shanghai alluvium are unlikely to exceed about 0.2 (e.g. see Lehane & Jardine 1994). K_i therefore evidently increases from a low value (i.e. less than K_o) at r=R to a maximum at r/R≈2 and then reduces to K_o at large radial distances from the pile. Such a trend is predicted by the Strain Path Method combined with the MIT-E3 soil model (Whittle & Baligh 1988) but cannot be reproduced using the CEM.

Measurements of the kind shown on Fig. 14 have not previously been reported and may be used directly to assess the predictive performance of various currently developing analytical/numerical approaches that model pipe pile installation.

CONCLUSIONS

Two open-ended pipe piles (A and B) were vibro-driven in a soft lightly overconsolidated clay deposit in Shanghai. These piles provide temporary formwork

for a newly patented large diameter cast-in-place concrete pipe pile, referred to as a PCC pile. Field instrumentation located at r/R $\geqslant 2$ recorded the surface ground displacements (surface heave and radial displacement), lateral deformations at depths, and also changes of stresses (pore water pressure and radial total stress) during the pile installation process. These measurements and a comparison with predictions made using the shallow strain path method (SSPM) and cavity expansion methods (CEM) indicated that, for r/R $\geqslant$2,

(i) Ground heave and lateral displacements at depth induced by pipe pile installation are well predicted using the SSPM (although the surface radial displacements at the test site were over-predicted due to the presence of a 2m surface layer of coarse grained fill).

(ii) The SSPM closed-form solution for the displacements at the ground surface for a closed-ended pile can be used for a pipe pile if the radius term in this solution is substituted by an equivalent radius (r_{eq}) corresponding to pile's annular end area.

(iii) The use of this same equivalent radius (r_{eq}) in cavity expansion method solutions for the excess pore pressure provides a simple means of assessing the excess pore pressure distributions around both pipe and closed-ended piles.

(iv) Maximum increases in lateral total stress in the vicinity of a displacement piles reduce systematically with r/r_{eq} and hence are also related to the displaced volume of the soil.

(v) Analagous to previously noted trends for the equalised lateral effective stress acting on the shaft of a full displacement pile, the Shanghai tests show that K_i reduces with the distance above the pile tip (h) and varies approximately with $(h/r_{eq})^{-0.3 \pm 0.1}$.

REFERENCES

Baligh M.M. (1985). Strain Path Method. *J. Geotech. Engng Div.*, ASCE, 111(9), 1101-1136.

Bond A.J. (1989). Behaviour of displacement piles in overconsolidated clays. Ph.D. Thesis, Univ. of London (Imperial College).

Butterfield R. and Bannerjee P.K. (1970). The effect of porewater pressures on the ultimate bearing capacity of driven piles. *Proc. 2nd Southeast Asian Conf. Soil Mech. & Fdn. Eng., Singapore,* 385-394.

Ghosh S. and Kikuchi N. (1991). An arbitrary Lagrangian-Eulerian finite element method for large deformation analysis of elastic-viscoplastic solid. *Comput. Meth, Appl. Mech. Engng*, 86, 127-188.

Gibson R.E. and Anderson W.F. (1961). *In situ* measurement of properties with the pressuremeter. *Civ. Engng Public Works Rev.* 56, 615-618.

Hu, Y. and Randolph M.F. (1998). A practical numerical approach for large deformation problems in soil. *Int. J. Numerical and Anal. Methods in Geomechanics*. 22, 327-350.

Jardine R.J. and Chow F.C. (1996). New design methods for offshore piles. MTD publication 96/103, Marine Technology Dept, London (publ.).

Kiousis P.D., Voyiadjis G.Z. and Tumay M.T. (1988). A large strain theory and its application in the analysis of the cone penetration mechanism. *Int. J. Numerical and Anal. Methods in Geomechanics*. 12, 45-60.

Lehane B.M. (1992). Experimental investigations of pile behaviour using instrumented field piles. Ph.D. Thesis, Univ. of London (Imperial College)

Lehane B.M. and Gill D.R. (2004) Displacement fields induced by penetrometer installation in an artificial soil. *Int. J. Physical Modelling in Geotechnics*,, 4(1), 25-37.

Liu H., Ma X. Chu H., Chen Y. And Gao Y. (2002a). Construction equipment for large diameter cast-in-place concrete pipe pile, ZL01273182X (patent)

Liu H., Ma X., Gong N. Fei K. And Hao X. (2002b). Construction technology for large diameter cast-in-place concrete pipe pile, CN1237296A (patent)

Lu Q., Randolph M.F., Hu Y. and Bugarski I.C. (2002). A numerical study of cone penetration in clay. Department of Civil and Resource engineering. University of Western Australia, Geomechnics Group, Research Report No. C:1681.

McCabe B.A. and Lehane B.M. (2003). Stress changes associated with driving pile groups in clayey silt. *Proc. XIII Eur. Conf. on Soil Mech and Fdn. Engng.*, Prague, 2, 271-276.

Pestana J.M. Hunt C.E. and Bray J.D. (2002). Soil deformation and excess pore pressure field around a closed-ended pile. *J. of Geotech. And Geoenv. Engineering*. ASCE, 128 (1), 1-12.

Randolph M.F. (2003). Science and empiricism in pile foundation design. *Geotechnique*, 53(10), 847-875.

Randolph M.F., Carter J.P. and Wroth C.P. (1979). Driven piles in clay – the effects of installation and subsequent consolidation. *Geotechnique*, 29(4), 361-393.

Randolph, M. F. 2003. Science and empiricism in pile foundation design. *Geotechnique*, 53(10), 847-875.

Roy M., Blanchet R., Tavenas F. and La Rochelle P. (1981). Behaviour of a sensitive clay during pile driving. *Canadian Geotechnical Journal*, 18(1),67-85.

Sagaseta C. (1987). Analysis of undrained soil deformation due to ground loss. *Geotechnique*. 37(3), 301-320.

Sagaseta C. and Whittle A.J. (2001). Prediction of ground movements due to pile driving in clay. *J. Geotech. And Geoenv. Engineering*, ASCE, 127(1), 55-66.

Sagaseta C., Whittle A.J. and Santagata M. (1995). Deformation analysis of shallow penetration in clay. Research Report R94-09, Massachusetts Institute of Technology.

Sagaseta C., Whittle A.J. and Santagata M. (1997). Deformation analysis of shallow penetration in clay. *Int. J. Numerical and Anal. Methods in Geomechanics*. 21, 687-719.

Van den Berg P., de Borst R. and Huetink H. (1996). An Eulerian finite element model for penetration in layered soil. *Int. J. Numerical and Anal. Methods in Geomechanics*. 20, 865-886.

Whittle A.J. and Baligh M.M. (1988). The behaviour of piles supporting tension leg platforms, final report Phase III. Dept. of Civil Engineering, Massachusetts Institute of Technology, USA.

Xu X. (2004). Numerical integration of shallow strain path method equations to deduce displacements due to pipe pile installation. Research Report XU/1/2004, School of Civil & Resource Engineering, University of Western Australia

Yu H.S., Herrmann L.R. and Boulanger R.W. (2000). Analysis of steady cone penetration in clays. *J. of Geotech. And Geoenv. Engineering*. ASCE, 126(7), 594-605.

Zienkiewicz O.C. (1984). Flow formulation for numerical solution of forming processes. In *Numerical Analysis of Forming Processes*, Wiley, New York, 1-44.

(a)

(b)

(c)

Figure 1 **(a) details of pile tip connection, (b) a group of completed PCC piles, and (c) installation of the pipe (formwork)**

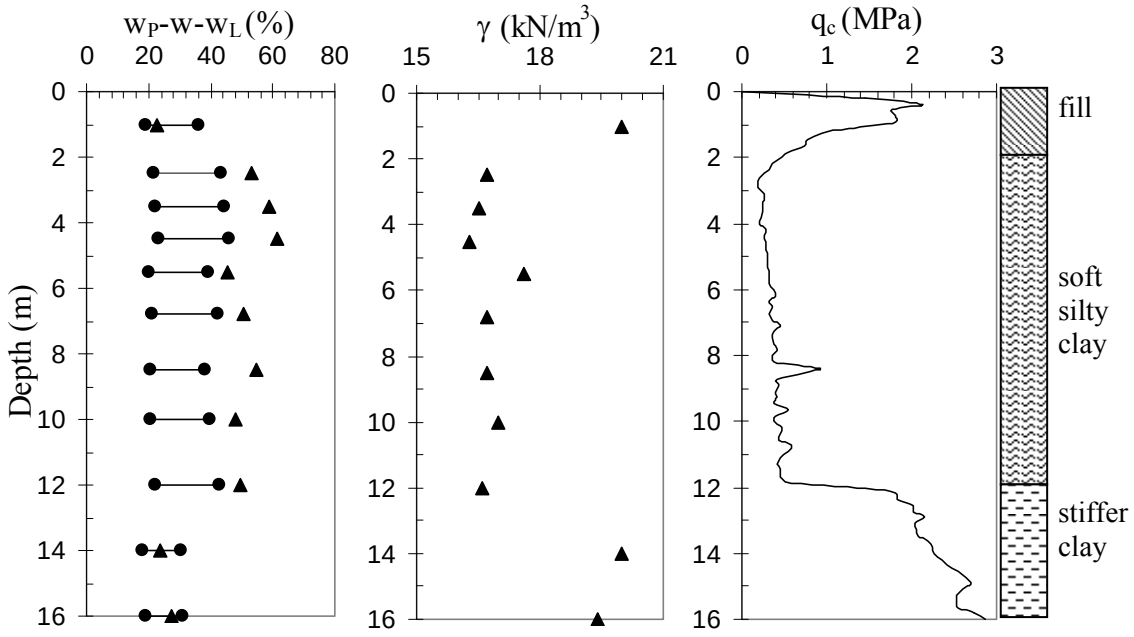

Figure 2 Site stratigraphy

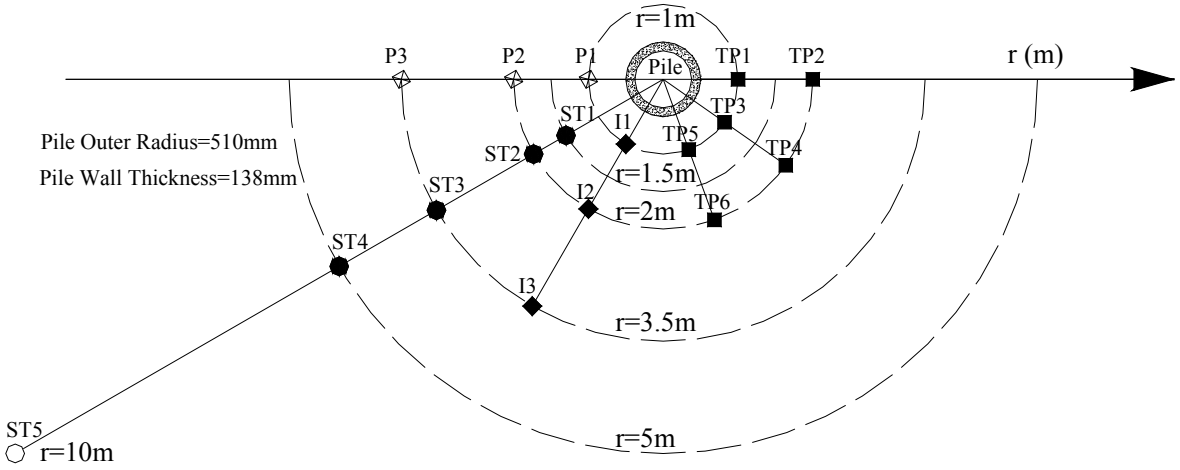

Figure 3 Instrumentation arrangement

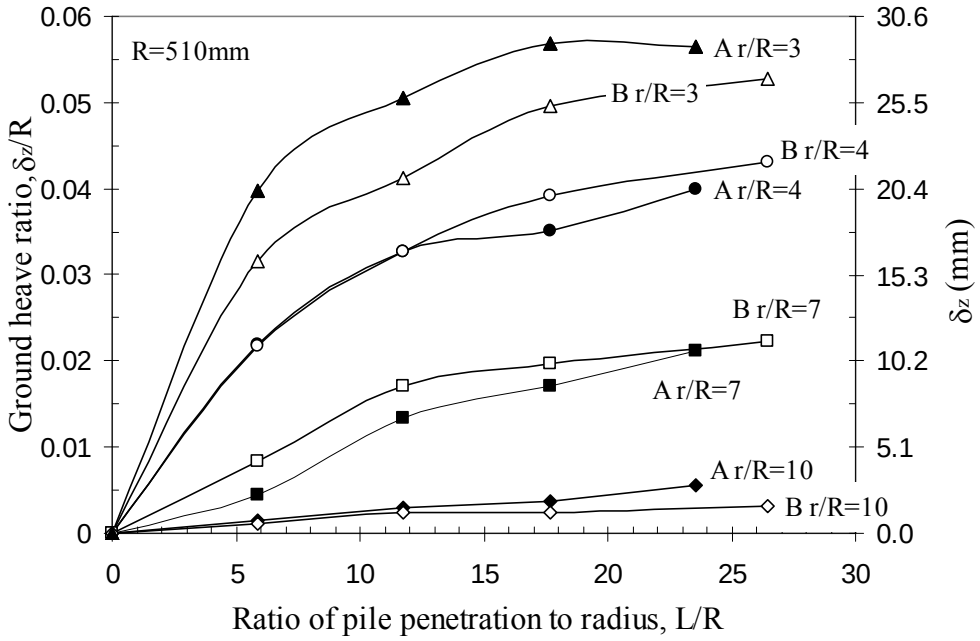

Figure 4 Ground heave development around Piles A and B

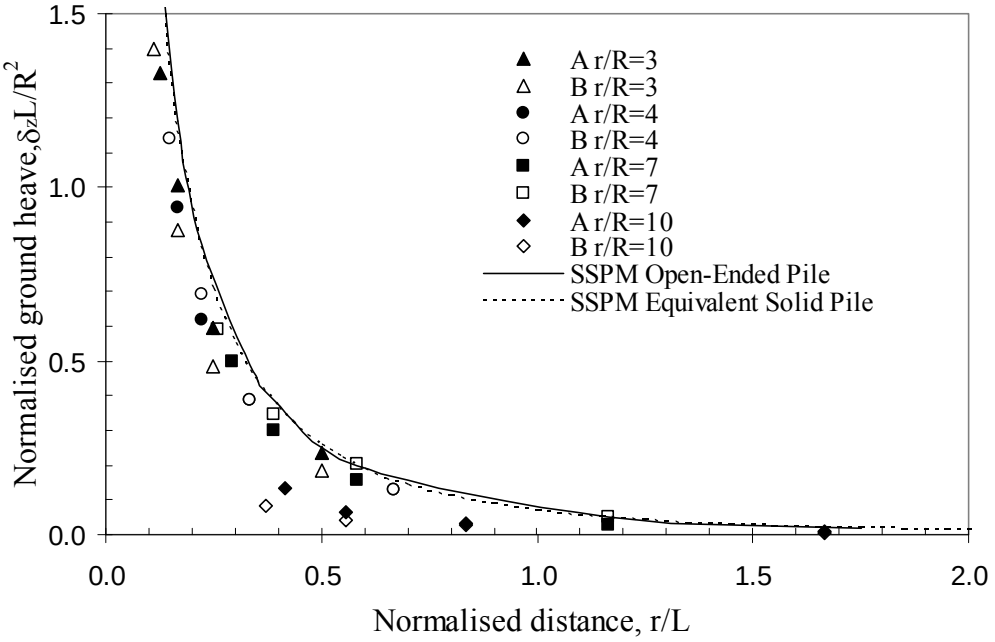

Figure 5 Ground heave: comparison of normalised field data with SSPM

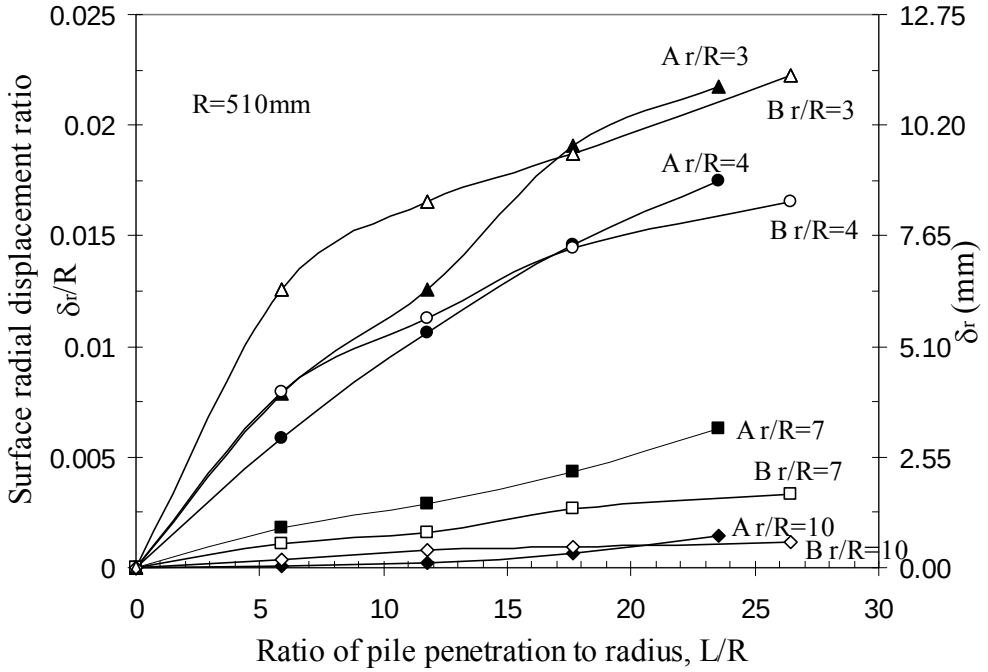

Figure 6 Surface radial displacement development for Piles A and B

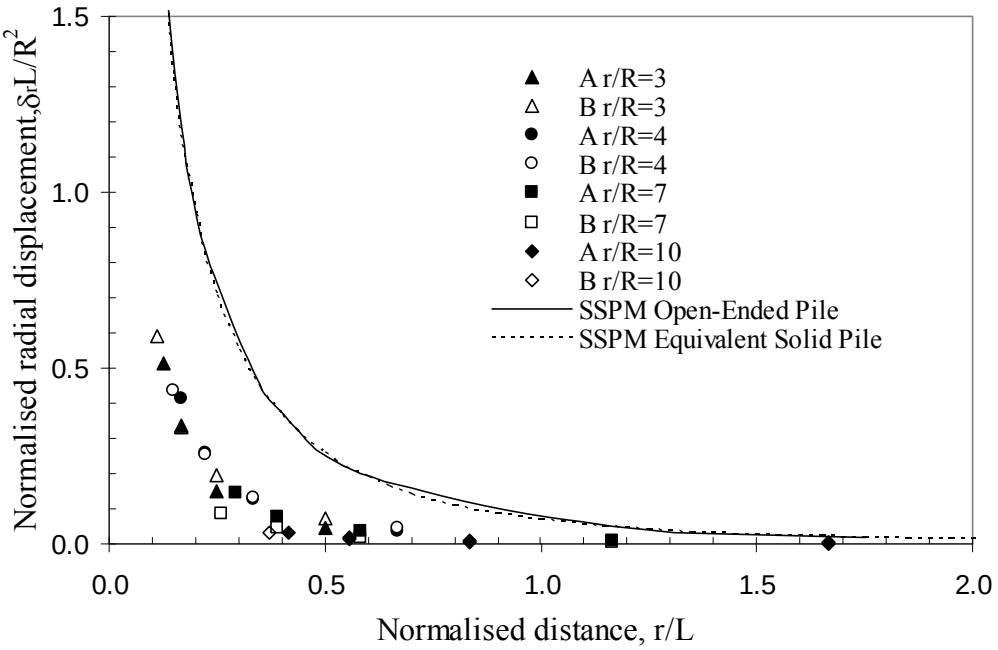

Figure 7 **Surface radial displacement: comparison of normalised field data with SSPM**

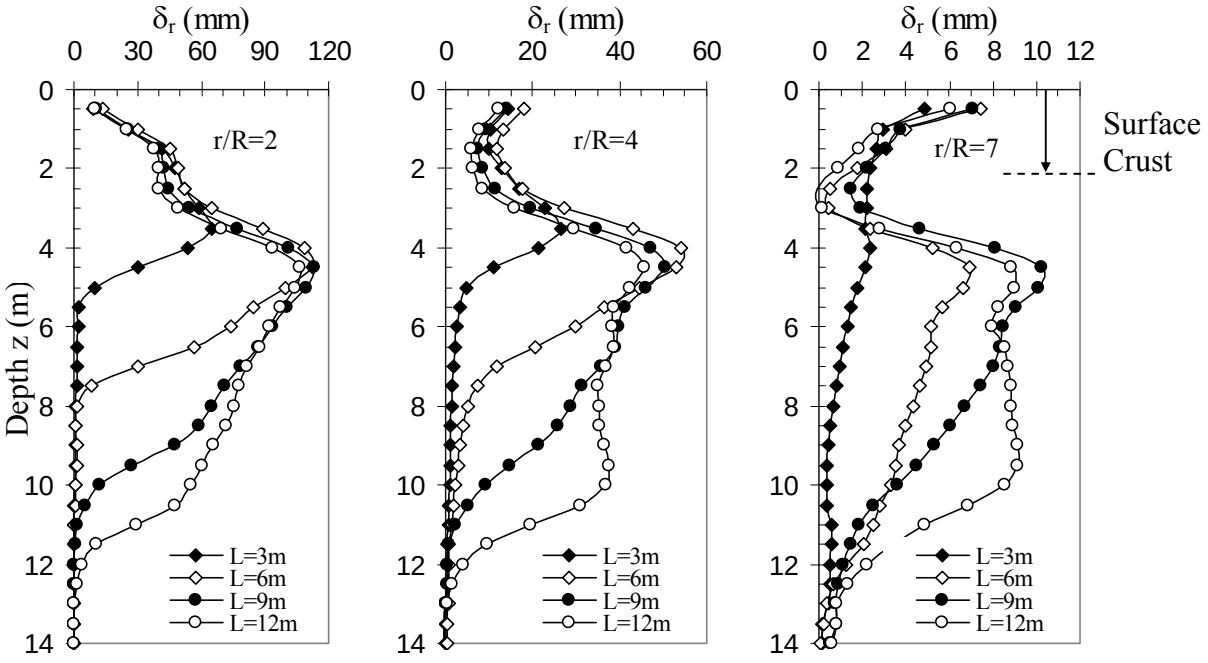

Figure 8 Measured lateral displacements at three radii

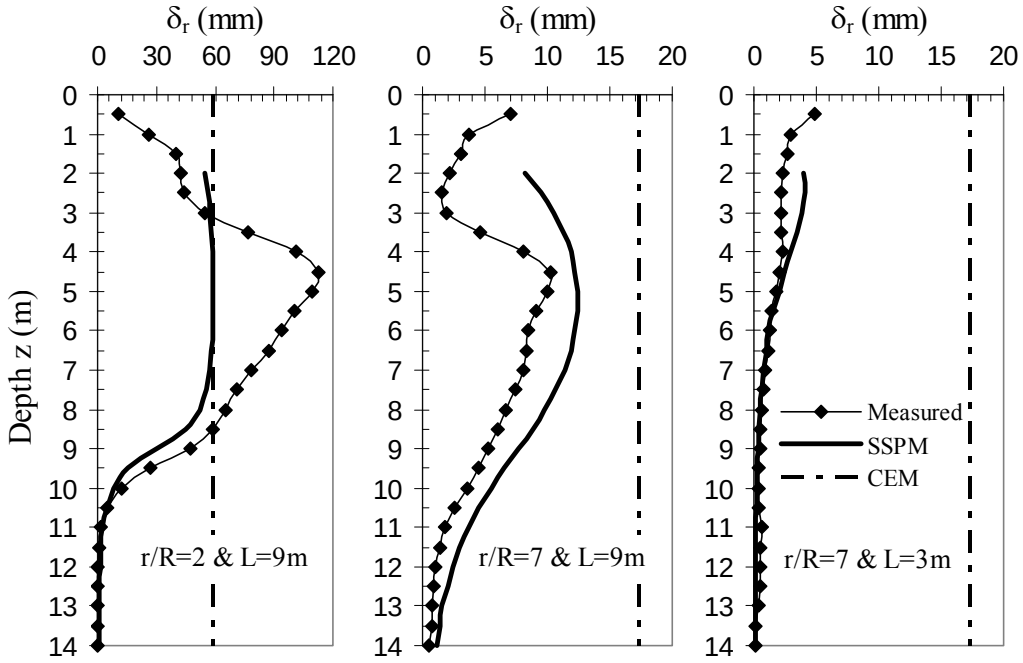

Figure 9 Comparison of measured δr data with SSPM and CEM

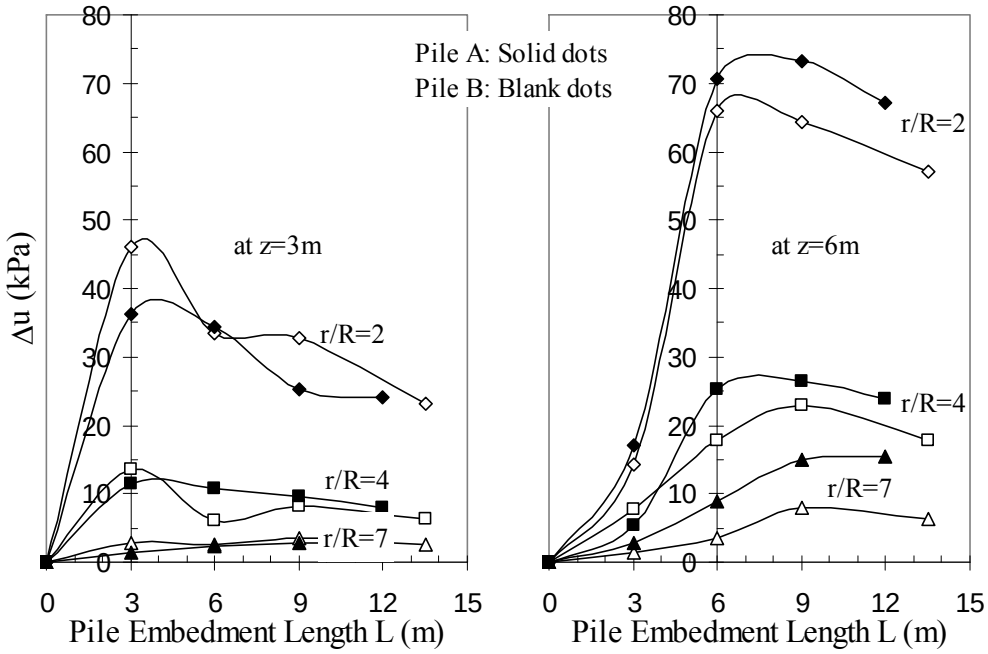

Figure 10 Excess pore water pressure due to pile installation

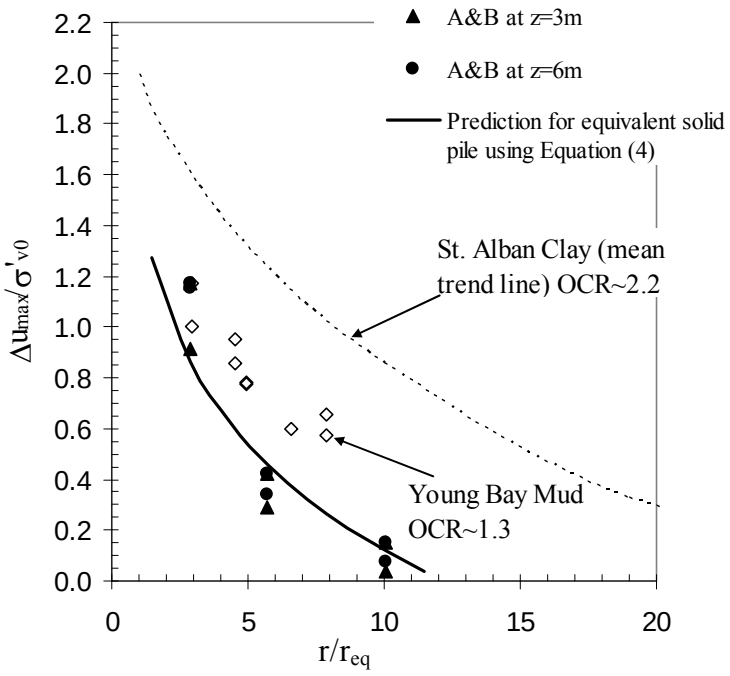

Figure 11 Radial distribution of excess pore water pressure, Δu_{max}

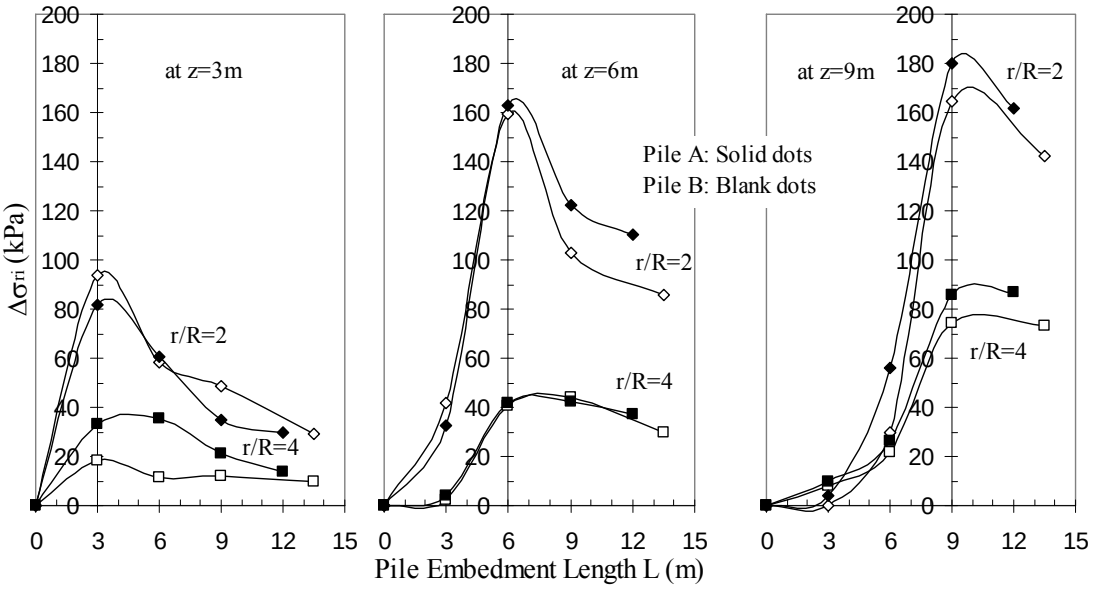

Figure 12 Radial total stress change due to pile installation

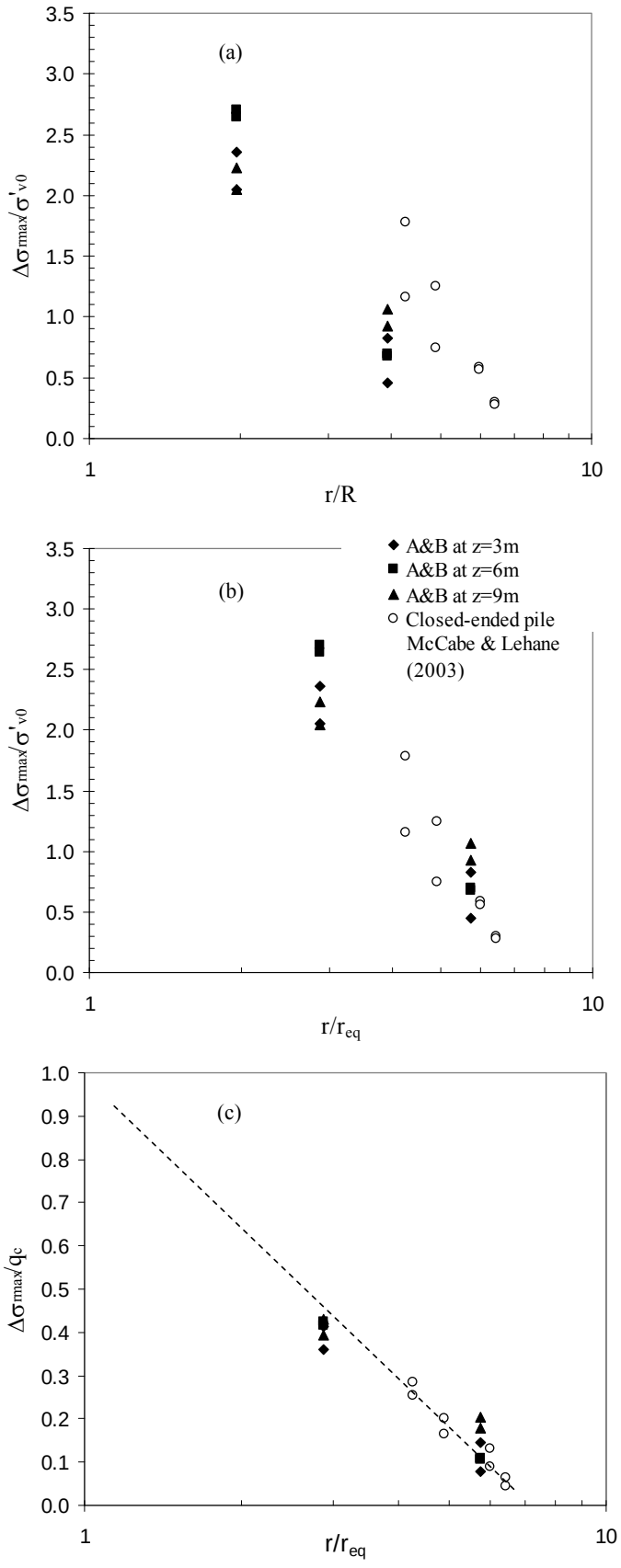

Figure 13 Radial distribution of radial total stress change, $\Delta\sigma_{rmax}$

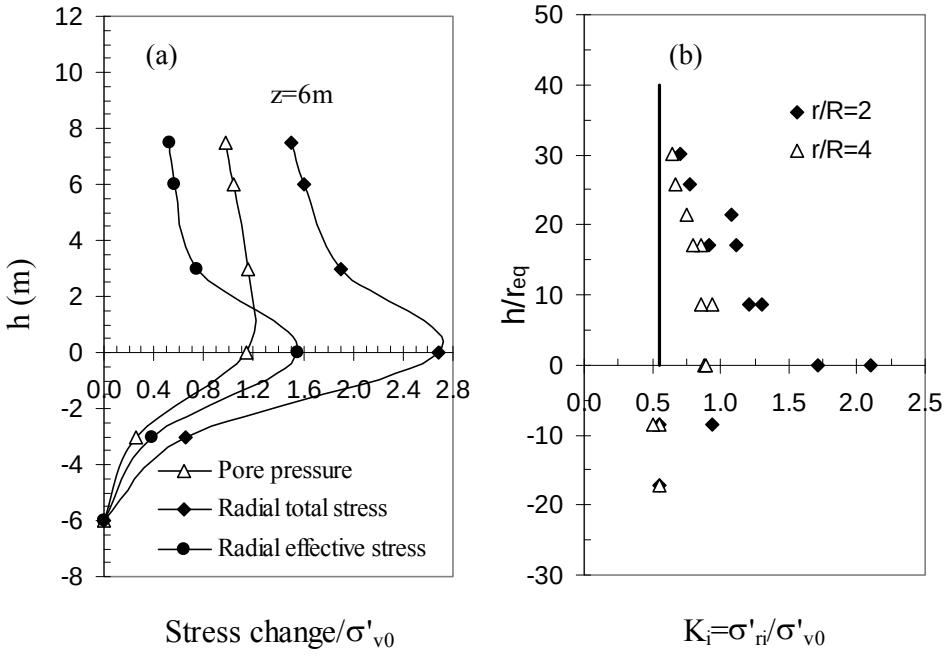

Figure 14 **(a) variation of stress change with h, and (b) variation of effective stress ratio K_i with h/r_{eq}**